APL Materials

All-silicon polarized light source based on electrically excited whispering gallery modes in inversely tapered photonic resonators

Cite as: APL Mater. **8**, 061110 (2020); https://doi.org/10.1063/5.0007759
Submitted: 16 March 2020 . Accepted: 26 May 2020 . Published Online: 18 June 2020

Sebastian W. Schmitt, Klaus Schwarzburg, George Sarau, Silke H. Christiansen, Sven Wiesner, and Catherine Dubourdieu

ARTICLES YOU MAY BE INTERESTED IN

Influence of post-deposition annealing on the photoelectrochemical performance of $CuBi_2O_4$ thin films
APL Materials **8**, 061101 (2020); https://doi.org/10.1063/5.0003005

Toward understanding and optimizing Au-hyperdoped Si infrared photodetectors
APL Materials **8**, 061109 (2020); https://doi.org/10.1063/5.0010083

Origins of infrared transparency in highly conductive perovskite stannate $BaSnO_3$
APL Materials **8**, 061108 (2020); https://doi.org/10.1063/5.0010322

© 2020 Author(s).

All-silicon polarized light source based on electrically excited whispering gallery modes in inversely tapered photonic resonators

Cite as: APL Mater. 8, 061110 (2020); doi: 10.1063/5.0007759
Submitted: 16 March 2020 • Accepted: 26 May 2020 •
Published Online: 18 June 2020

View Online
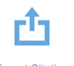
Export Citation

CrossMark

Sebastian W. Schmitt,[1,a)] Klaus Schwarzburg,[2] George Sarau,[3,4] Silke H. Christiansen,[3,4,5,b)] Sven Wiesner,[1] and Catherine Dubourdieu[1,6,a)]

AFFILIATIONS

[1] Institute Functional Oxides for Energy-Efficient Information Technology, Helmholtz-Zentrum Berlin für Materialien und Energie, Hahn-Meitner Platz 1, 14109 Berlin, Germany
[2] Institute for Solar Fuels, Helmholtz-Zentrum Berlin für Materialien und Energie, Hahn-Meitner Platz 1, 14109 Berlin, Germany
[3] Renewable Energy Division, Helmholtz-Zentrum Berlin für Materialien und Energie, Hahn-Meitner Platz 1, 14109 Berlin, Germany
[4] Max Planck Institute for the Science of Light, Staudtstrasse 2, 91058 Erlangen, Germany
[5] Physics Department, Freie Universität Berlin, Arnimallee 14, 14195 Berlin, Germany
[6] Physical Chemistry, Freie Universität Berlin, Arnimallee 22, 14195 Berlin, Germany

[a)] **Authors to whom correspondence should be addressed:** sebastian.schmitt@helmholtz-berlin.de and catherine.dubourdieu@helmholtz-berlin.de
[b)] **Now at**: Fraunhofer Institute for Ceramic Technologies and Systems IKTS, Winterbergstrasse 28, 01277 Dresden, Germany.

ABSTRACT

As a result of its indirect bandgap, emitting photons from silicon in an efficient way remains challenging. Silicon light emitters that can be integrated seamlessly on a CMOS platform have been demonstrated; however, none satisfies an ensemble of key requirements such as a small footprint, room-temperature operation at low voltages, and emission of narrow and polarized lines with a high spectral power density in the near-infrared range. Here, we present an all-silicon electrically driven light emitting diode that consists of an inversely tapered half-ellipsoidal silicon photonic resonator containing a p–n junction used to excite whispering gallery modes (WGMs) inside the resonator. Under low voltage operation at room temperature, such a photonic silicon light-emitting diode exhibits a band-edge emission (900–1300 nm) with a wall-plug efficiency of 10^{-4}. The emitted spectrum is amplified in multiple WGMs and shows peaks that are polarized and have linewidths $\Delta\lambda$ as narrow as 0.33 nm and spectral power densities as high as 8 mW cm^{-2} nm^{-1}. Considering its small footprint of ~1 μm and remarkable emission characteristics, this silicon light source constitutes a significant step ahead toward fully integrated on-chip silicon photonics.

© 2020 Author(s). All article content, except where otherwise noted, is licensed under a Creative Commons Attribution (CC BY) license (http://creativecommons.org/licenses/by/4.0/). https://doi.org/10.1063/5.0007759

I. INTRODUCTION

Integration of III–V semiconductors by bonding or epitaxial growth has brought remarkable progress toward small footprint and CMOS-compatible on-chip optical emitters. However, the use of costly materials and complex processing impedes a breakthrough toward the mass production of fully integrated light sources on chips.[1–3] Silicon light emitters remain the ultimate solution to this problem, but even though silicon is a well-established photonic material for passive applications, its bandgap is indirect and the design of silicon light emitters remains a challenging task.[4,5]

Multiple research routes have been explored to increase the optical efficiency of silicon. Experiments on quantum confinement in silicon nanostructures could demonstrate optical gain,[6,7] and enhanced sub-band-edge light emission in silicon could be triggered by dislocation loops,[8] structural defects (so-called “A” or “W”

centers),[7,9] or via the doping of silicon with erbium, hydrogen, or copper.[10–14] Furthermore, the enhancement of the local density of optical states (LDOS) by optimized ray-optical or by photonic light trapping was used to amplify spontaneous emission rates of silicon band-edge emission and the emission of optically active defects.[13–18] By the excitation of photonic modes in silicon optical resonators with high energy electron beams, a spectrally selective amplification of cathodoluminescence (1000–1600 nm) could be reached.[19,20] Another recent work could demonstrate an enhanced light emission from silicon by controlling its electronic spin properties in strong magnetic fields.[21] Despite these successes, all presented approaches do not simultaneously meet the requirements for high resolution on-chip sensing devices, efficient integrated optical links, or photonic computing architectures.[22–26] In particular, in addition to a small footprint and small emission spot, these comprise a low voltage room-temperature emission of narrow and polarized spectral lines with a very high spectral power density. As a matter of fact, Si-light-emitting diodes (LEDs) reported so far are still quite large, require a relatively high operation voltage, or have an unpolarized broadband emission and low spectral power densities,[8,9,13,15,27–31] as summarized in the supplementary material, Table ST1. Prototypes including silicon nanocrystals, even though they appear scalable and have so far the highest quantum efficiencies, are characterized by relatively broad, unpolarized, and blue shifted emission spectra between 600 nm and 800 nm.[32] Si-LEDs fabricated from optically doped photonic crystals could reach small footprints (~25 μm^2) and sharper emission lines (~1 nm) with a higher spectral output power density; however, they still suffer from very low wall-plug efficiencies of about 10^{-8}.[13] The present study goes one step ahead in small scale Si-LED design. Starting from the concept of on-chip inversely tapered photonic resonators with a footprint of ~1 μm^2 that we previously described in detail in Ref. 19, we directly integrated a p–n junction into these resonators. Due to the direct electrical excitation of silicon band-edge radiation in high quality (Q) factor photonic resonators, we can demonstrate a monolithically integrated Si-LED device with an unprecedented small size and spectral emission properties. The spectral output is characterized by sharp (0.33 nm) and polarized emission lines between 900 nm and 1300 nm, a very high output power density and spectral output power density ($6 \cdot 10^5$ μW cm^{-2} and $8 \cdot 10^3$ μW cm^{-2} nm^{-1}, respectively) in combination with a relatively high quantum efficiency (10^{-5}) and wall-plug efficiency (10^{-4}).

II. ALL-SILICON LIGHT EMITTING DIODE DEVICE CONCEPT AND FABRICATION

Figure 1(a) shows a typical scanning electron microscope (SEM) image of a Si-LED under study. Its design is based on the combination of an inverted-tapered silicon resonator together with a p–n junction inserted inside the resonator. The optical properties of inversely tapered silicon photonic resonators have been recently investigated in close detail using cathodoluminescence (CL), photoluminescence (PL), and numerical simulations[18,19] and are dramatically different from the ones of a straight Si nanowire. Upon excitation with visible light, a straight nanowire emits a broad near-infrared (NIR) luminescence spectrum. An inversely tapered Si nanostructure, as shown in Fig. 1(a), shows multiple emission peaks with a strongly enhanced integral band-to-band luminescence (up to 200-fold).[18,19] We showed that these inversely tapered silicon structures host a multitude of hybrid optical modes, which consist of whispering gallery modes (WGMs) in orbits of discrete heights that are superimposed with a Fabry–Perot-like branch along the z-axis. Figure 1(b) displays numerical finite difference time domain (FDTD) simulations of the relative cross sectional energy density (E^2) in x–y (top) and x–z directions (bottom) for several of the photonic modes confined in the Si-resonator shown in Fig. 1(a) (see the details on FDTD simulations in the supplementary material). Modes were found to be polarized along the z-axis of the resonators or in the x–y plane and their formation is closely linked to the geometrical shape of the inverse taper, e.g., inverted cone or inverted half ellipsoid.[19] The strong enhancement of the individual emission lines is attributed to the large Purcell factors of the WGMs.[18,33] By inserting a p–n junction into the resonator, we propose to electrically excite the silicon band-edge radiation to produce the narrow light emission from the inversely tapered Si resonator. In this way, the device, as shown in Fig. 1(a), is an on-chip integrated electrically driven light source.

The details of the whole fabrication process are given in the supplementary material. Briefly, the photonic resonators are fabricated by cryogenic reactive ion etching (RIE) of a silicon wafer using silica sphere lithography. Tuning of the RIE process parameters permits us to control the shape of the inverse taper. The design presented here exhibits an ellipsoidal taper, which was chosen, as it hosts more optical modes than the shape of an inverse conical taper with a comparable structure height, as we previously showed.[19] In the device shown in Fig. 1(a), the ellipsoidal long axis has a length of 3342 nm, while the short axis has a length of 424 nm. To introduce a p–n junction into the resonators, the RIE process was performed on a wafer with a doping profile designed such that the p–n junction is situated inside the photonic resonator, at a distance from the top of about 750 nm [see Figs. 1(a) and 1(b)], whereas the top and substrate of the structure are degenerately doped (n++ and p++, respectively) to serve as contacts for the electrical connection of the Si-LEDs [see Fig. 1(a)].[34]

Electrical and electroluminescence (EL) measurements on the Si-LEDs were performed in an atomic force microscope (AFM) with a tungsten coated silicon probe that served as a top contact. To collect EL emission, a dc forward bias was applied via the AFM probe and a 100× VIS objective was focused onto the contacted Si-LED at an angle of 65° to the z direction. Photoluminescence (PL) emission of the Si-LEDs was excited (632 nm HeNe cw laser) and collected along the z direction with a 50× VIS–NIR objective in an optical microscope. EL and PL emissions were analyzed using a VIS–NIR optical spectrometer. Figure 1(c) shows the top view of the sample in an optical microscope, while Fig. 1(d) displays an AFM scan of the exact same surface region. The zoom from the AFM scan indicates the Si-LED shown in Fig. 1(a). In both the AFM and SEM images, a tungsten deposit on top of the Si-LED originating from the electrical contact with the AFM probe is clearly visible. The details on the experimental setup and the treatment of the spectral data are provided in the supplementary material.

III. DIODE ELECTRICAL CHARACTERIZATION

To assess the electrical properties, I–V measurements were performed on individual Si-LEDs. Figure 2(a) displays a

© Author(s) 2020

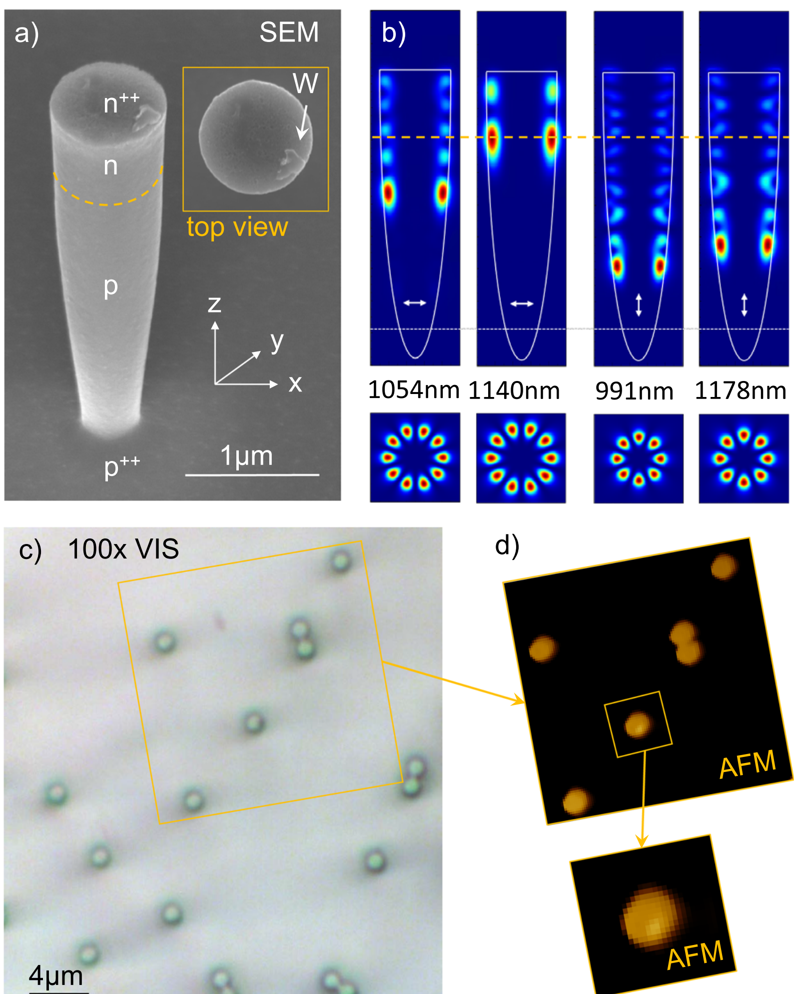

FIG. 1. (a) SEM image showing a 45° inclined view of a Si-LED and a view of the top facet (inset). Letters indicate the doping profile of the structure (phosphorous doping for n, boron doping for p) and the position of the tungsten deposited from the electrical contact with the AFM cantilever (W tip). Directions x and y define the planes parallel to the substrate while z is the direction normal to it. The dashed yellow line indicates the position of the p–n junction. (b) Numerical FDTD simulations of the relative cross sectional energy density (E^2) in x–y (top) and x–z (bottom) planes for four exemplary photonic modes confined in the Si-LED (1054 nm and 1140 nm both x–y polarized, 991 nm and 1178 nm both z polarized). The white arrows indicate the polarization direction of the visualized modes. Curved white lines indicate the projected (half-ellipsoidal) geometry of the resonator, and the horizontal line indicates the position of the substrate. As in panel a) the dashed yellow line indicates the position of the p–n junction. (c) Top overview images of the sample from optical microscopy (100× VIS) showing the position of various Si-LEDs on the silicon substrate. (d) AFM scan after the EL measurement and a zoomed-in view of the device shown in (a).

semi-logarithmic plot of the current measured in the Si-LED shown in Fig. 1(a) in the voltage range ±2.5 V. It can be seen that the diode exhibits an obvious rectifying behavior and is characterized by a low reverse leakage current and a relatively high series resistance in the forward direction. I–V measurements performed on different Si-LED devices lead to similar data with only a very low variability (see the supplementary material, Fig. S7). The electrical characteristics of the devices can be simulated using the equivalent circuit model that is shown in Fig. 2(a) (inset); it consists of a Shockley diode with a contact series resistance R_s and a reverse leakage current I_D, flowing over an ohmic parallel resistance R_p. The relation between the current I and the applied voltage U is given as follows:

$$I = I_o \cdot \left[\exp\left(\frac{U + IR_s}{nU_T}\right) - 1\right] - \frac{U + IR_s}{R_p}. \qquad (1)$$

The first term in Eq. (1) represents the diode current I_D in which I_o, R_s, U_T, and n indicate the saturation current, series resistance, thermal voltage, and ideality factor of the diode, respectively, while the second term represents the current over the parallel resistance R_p. Fitting the experimental I–V data using Eq. (1) permits us to quantify the electrical properties of the individual Si-LEDs. For the data shown in Fig. 2(a), we find a very low saturation current I_o of 1.6 pA [which translates to a saturation current density of ~10^{-3} A/cm^2 considering the cross section of the bottom of the diode—see Fig. 2(a), right axis] and a parallel resistance R_p as high as 7.0×10^{12} Ω, revealing that the second term in Eq. (1) is very small. Physically, this means that even though the Si-LED has a very high surface to volume ratio, leakage currents over the surface do not significantly contribute to the diode characteristics, i.e., the native oxide covering the surface provides a robust electrical passivation (see the supplementary material on the formation of the surface oxide). Furthermore, we find a series resistance R_s of 17 kΩ that is predominantly caused by the small AFM contact area. The product nU_T is found to be 45 mV, allowing for reasonable values of the diode ideality (1–1.5) and the thermal voltage (25 mV at 25 °C–45 mV at 250 °C) for the diode under operation conditions. Figure 2(b) [zoomed-in image of Fig. 2(a)] shows the Si-LED current in the operational

© Author(s) 2020

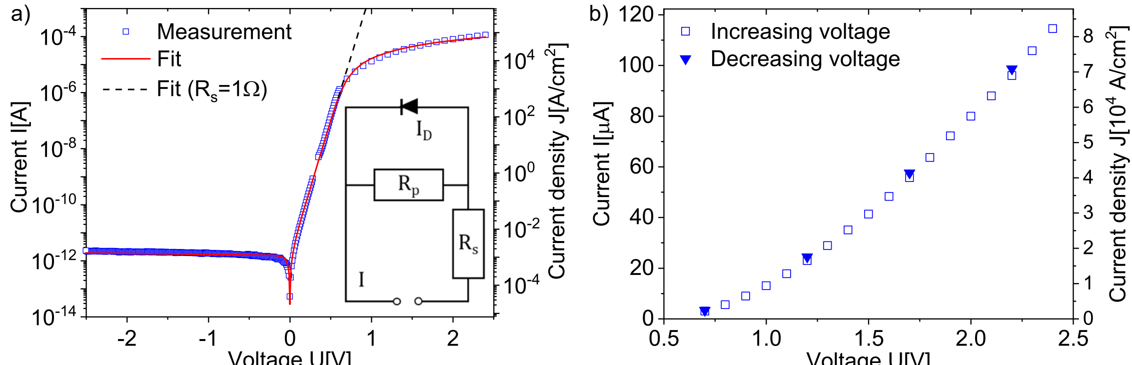

FIG. 2. (a) Semi-logarithmic plot of the I–V characteristics of the Si-LED. Blue rectangles are the measured values, while the red line indicates a fit with Eq. (1) that describes the equivalent circuit of the Si-LED device depicted in the inset. Here, R_p, R_s, I_D, and I indicate the parallel resistance, series resistance, diode current, and total current, respectively. The black dashed line indicates the evolution of the diode current for a series resistance of R_s = 1 Ω. (b) Zoomed-in view of the I–V characteristics of the Si-LED in linear scale in the voltage range in which the EL measurements are done. The solid triangles indicate data from the measurement with decreasing applied voltage steps. In both plots, the right axis shows the current density calculated with respect to the cross section of the bottom of the Si-LED.

voltage range between 0.5 V and 2.5 V. Measurements with reversed voltage steps (decreasing voltage) performed after about 1 h show the stability of the contact provided by the AFM tip. Current densities of up to almost 10^5 A/cm^2 [see Fig. 2(b), right axis] do not affect the structure of the Si-LEDs as indicated by Raman measurements that provide the same result before and after operation (see the supplementary material, Fig. S5). A review of the analyzed electronic properties shows that the used fabrication processes permit us to create silicon diodes of an outstanding quality with only minor parasitic currents occurring in the electrical pumping of the device. The diode operation could still be improved by optimizing the contact formation with the AFM cantilever, which causes a resistive loss. The dashed line in Fig. 2(a) indicates the evolution of the diode current fit function when a much lower series resistance R_s of 1 Ω is considered instead of the actual one of 17 kΩ. It shows that, with a much lower series resistance, the LED could be operated below 1 V.

IV. ELECTROLUMINESCENCE PROPERTIES—COMPARISON WITH PHOTOLUMINESCENCE

Figure 3(a) shows the EL emission spectrum of the Si-LED shown in Fig. 1(a) measured at room temperature at a forward bias of 1.7 V [which corresponds to a drive current of 57 μA and a power of 97 ± 5 μW; see Fig. 2(b)]. The spectrum is centered around the silicon band-edge emission (1100 nm) and extends between about 950 nm and 1300 nm. Furthermore, it shows a multitude of sharp emission peaks, originating from the light amplification by photonic modes hosted inside the inversely tapered device [see Fig. 1(b)].[18,19] Note that spectrally close peaks do not correspond to mode splitting, but to a superposition of different modes in the resonator spectra. For comparison, PL measurements were performed using a 632 nm cw laser excitation at a power of 85 ± 5 μW. Figure 3(b) displays the PL emission of the Si-LED shown in Fig. 1(a). On all measured devices, the PL spectra show similar photonic peaks than the EL ones but on average have a lower intensity [see zoomed spectra of Figs. 3(c) and 3(d) and also the superpositions of Figs. 3(a) and 3(b) and of Figs. 3(c) and 3(d) in the supplementary material, Fig. S10]. Missing or faint peaks in the PL spectrum cannot be attributed to changes in the free spectral range (FSR) between the cases of electrical and optical pumping since the same resonator is measured with a comparable input pump power (comparable density of free carriers). Instead, the electrical pumping leads to a more efficient excitation of the photonic modes in the Si-LEDs as compared to optical pumping.

The WGMs are most efficiently excited by the p–n junction when they have a spatial overlap with its position and a spectral overlap with its emitted spectrum (silicon band-to-band emission at room temperature, between 950 nm and 1250 nm). In the device under study, these requirements are well fulfilled by the 1140 nm mode shown in Fig. 1(b). It shows a spatial overlap with the position of the p–n junction and has a wavelength close to the band emission maximum in silicon of about 1100 nm. In Fig. 3(a), it can be seen that the mode, indeed, shows the highest light emission in the EL measurements. Since mode properties (wavelength, polarization, spatial position, and effective refractive index) in the resonator depend on its shape and dimensions,[19] the emission efficiency and output coupling of the Si-LED modes can be tuned by changing these parameters and/or the location (height) of the p–n junction in the resonator through the fabrication process. While the geometry of the resonator can be influenced by the RIE parameters, the relative height of the p–n junction in the resonators can be adjusted by the RIE time and by the p–n-junction depth in the substrate wafer before etching.

Integrating the absolute emission counts from Figs. 3(a) and 3(b) and comparing them to the electron/photon pumping flux, we find that the Si-LEDs under study exhibit quantum efficiencies (QE) of about 1×10^{-5} for electrical and about 5×10^{-6} for optical excitation (details on the optical measurements and the calibration of the spectra are given in the supplementary material; note that the optical and electrical excitation powers are quite similar). The differences in

© Author(s) 2020

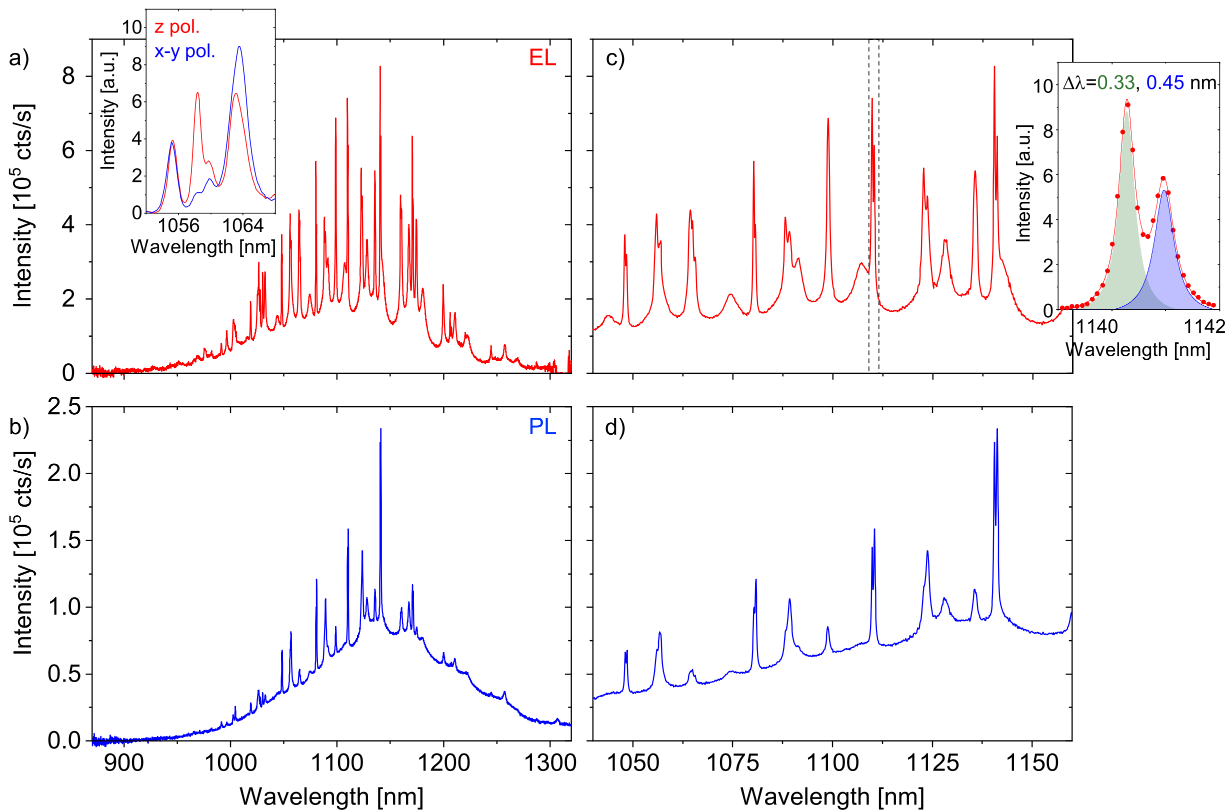

FIG. 3. (a) EL spectrum of an individual Si-LED [as shown in Fig. 1(a)] excited with an electrical power of 97 μW. The inset shows an example of spectral lines measured with respect to z and x–y polarization. (b) PL spectrum of the same Si-LED excited with a 632 nm cw laser at a power of 85 μW. (c) Zoomed-in spectrum of the graph shown in panel (a) in the spectral range 1040–1160 nm. The dashed vertical lines indicate the spectral range shown in the inset. The inset depicts two spectral lines fitted with a Voigt profile (green and blue lines: fit functions, red points: measured spectral data, and red line: sum of the two fit functions). Δλ indicates the linewidth. (d) Zoomed-in spectrum of the graph shown in panel (b) in the spectral range 1040–1160 nm.

mode excitation efficiency and overall quantum efficiency occur due to the fact that only about 50% of the 632 nm laser can be coupled to the structure during the PL measurements in the back-scattering configuration. The QE of about 1×10^{-5} can be converted to a so-called "wall-plug efficiency" of 2×10^{-4} calculated by the emitted photon power (0.007 μW) divided by the applied power of 1.7 V $\times$ 57 μA = 97 μW. As compared to the only other Si-LED device which involves the integration of an optical resonator for a photonic modification of the diode emission spectrum, this wall-plug efficiency is about 4 orders of magnitude larger.[13]

According to the numerical FDTD simulations, photonic modes hosted by the Si-LEDs are polarized along the z direction or in the x–y plane [see Figs. 1(a) and 1(b)] and have Q-factors $>10^3$, which result in emitted spectral lines with widths below 1 nm.[18,19] As can be seen in the inset of Fig. 3(a), the mode polarization is partly retained in the mode emission observed under 65° to the z-axis (see also the supplementary material, Fig. S6). Note that even though the Si-LEDs emit light in z and x–y directions, due to the rotational symmetry of the constituting resonator structures [see Fig. 1(a)], the light emitted along the z direction cannot be linearly polarized. Furthermore, by fitting of the modes λ with Voigt profiles,[35] we could confirm linewidth Δλ as narrow as 0.33 nm [see the inset of Fig. 3(c)] and quality factors Q = Δλ/λ that reach $\sim 4 \cdot 10^3$. For a given pumping current, the intensity of the emission spectra, QE, and spectral linewidth of the modes were comparable for different Si-LED devices on the sample. Occurring differences can be explained by an unintentional geometrical variability (slightly varying resonator shape/dimensions or surface roughness) of the devices in the fabrication process, which acts on the mode formation in the Si-LEDs (see the comparison of spectra from different Si-LEDs in the supplementary material, Fig. S8).[19]

A spectral linewidth of 0.33 nm and a polarized emission are unique features of the presented device and to the best of our knowledge could so far not be shown for a Si-LED. In previously demonstrated large area all-silicon devices based on bulk silicon and silicon nanocrystals, the emitted light is not polarized and has a spectral linewidth between 50 nm and several 100 nm.[8,15,23,29,30,32] For an all-silicon diode based on a photonic crystal, linewidths as narrow as ~1 nm could be shown; however, a polarized emission was not reported.[13] While wall-plug efficiencies for some bulk Si-LEDs are about two orders of magnitude larger,[15] the photonic Si-LED in this work outperforms the only so far reported all-silicon LED based on

© Author(s) 2020

a photonic cavity by about four orders of magnitude.[13] The relatively high output intensity at small voltages I, the small emission spot area A of ~1 μm^2 (supplementary material, Fig. S2), and very narrow linewidth $\Delta\lambda$ result in an output power density I/A and a spectral output power density $I/(A\cdot\Delta\lambda)$ as high as 600 mW cm^{-2} and 8 mW cm^{-2} nm^{-1}, respectively (e.g., from the mode at 1140.3 nm in Fig. 3). Since all-Si LED devices reported so far have a large area emission spot and very broad linewidth[8,15,29,30] (supplementary material, Table ST1), these values can only be compared to the ones of a photonic silicon emitter, which only reach substantially lower values of 4×10^2 μW cm^{-2} and 8×10^2 μW cm^{-2} nm^{-1}, respectively.[13] Furthermore, the operating voltage and power of the device are very low, as compared to the majority of Si-LED technologies (supplementary material, Table ST1).[8,9,15,27–30,32]

V. POWER DEPENDENCE OF THE ELECTROLUMINESCENCE

The dependence of the spectral emission of the Si-LEDs on the pumping power is further analyzed in Figs. 4(a)–4(d). Figure 4(a) depicts an intensity map of the spectral power dependence in the emission range 1078–1112 nm of the Si-LED shown in Fig. 1(a). We observe that with rising power between 0 μW and about 300 μW [the I–V curve in the operational range is plotted in Fig. 2(b)], the emission peaks emerge from the spectra. For the different pumping powers, the three peaks indicated in the map were fitted using a Voigt profile, and the fit parameters—peak amplitude, peak position, and peak width—are plotted in Figs. 4(b)–4(d), respectively.[35] Figure 4(b) shows a double logarithmic plot of the power dependence of the three peak amplitudes. It is found that the peak intensity increases almost linearly with the applied power over more than two orders of magnitude. The peak positions exhibit a slight redshift [Fig. 4(c)] of typically ~1 nm over the power range 0–300 μW. Most likely, this can be attributed to heating of the Si-LED under operation. Temperature changes can affect the mode wavelength in a photonic resonator in two ways since both the refractive index and the lattice constant of the material are temperature dependent. In the presented Si-LED, it can be estimated that the variation of the resonance wavelength caused by the thermal gradient of the refractive index is at least one order of magnitude larger than the one caused by the thermal expansion.[36,37] From the temperature gradient of the

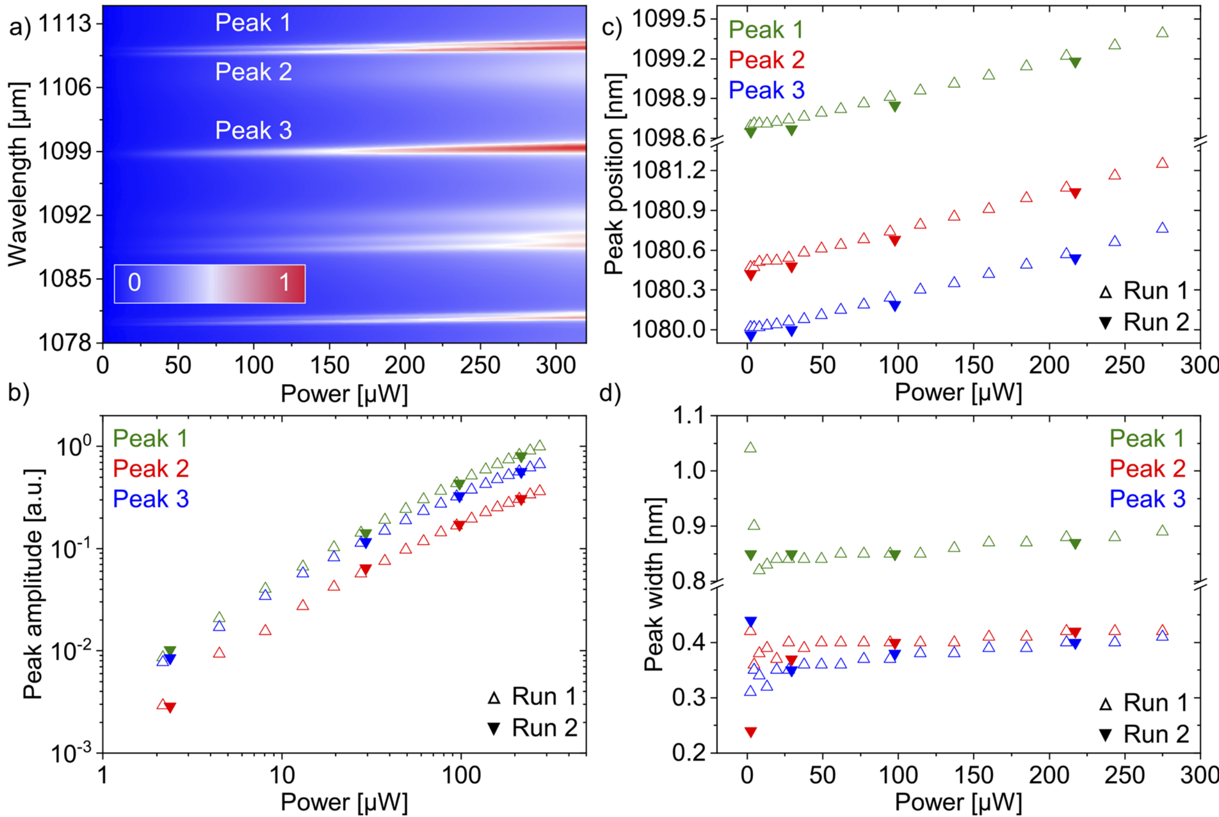

FIG. 4. (a) Intensity map showing the power dependence of the EL spectrum of the individual Si-LED shown in Fig. 1(a). Three peaks are indicated for further discussion in panels (b)–(d). Open and full triangles indicate the first and second measurements as in Fig. 2(b). (b) Double logarithmic plot of the amplitude vs power of the three peaks indicated in (a). (c) Power dependence of the peak position for the three peaks indicated in (a). (d) Power dependence of the peak width for the three peaks indicated in (a).

© Author(s) 2020

silicon refractive index dn/dT = 10^{-4} K^{-1}, it can be derived that the diode heats only by about 10 K over the entire excitation power range, indicating that most heating occurs in the series resistance at the contact (see the detailed discussion on the electrical properties of the diodes above), and, therefore, does not significantly affect the modes. Furthermore, assuming a heating of only about 10 K and considering the fitting results of the LED characteristics, we can now specify the ideality factor of our device as about 1.7. As shown in Fig. 4(d), the emission lines exhibit widths $\Delta\lambda < 1$ nm that are almost constant over the entire driving power range. Values in Figs. 4(b)–4(d) were found to be reproducible in a second measurement run performed 1 h after the first one.

VI. SUMMARY AND CONCLUSIONS

In summary, we propose a new type of electrically driven all-silicon light emitter with a ~1 μm footprint, monolithically integrated on a silicon wafer. A p–n junction is inserted into a silicon photonic resonator, consisting of an inverted-tapered half-ellipsoid-shaped pillar, which hosts a multitude of polarized whispering gallery modes distributed along its height. The spectral output of the resulting light emitting diode is characterized by a low voltage operation (1.7 V), sharp ($\Delta\lambda < 1$ nm) polarized emission lines between 900 nm and 1300 nm, which originates from the amplification of electrically pumped (via the p–n junction) silicon band-edge radiation in the photonic modes of the resonator. Resulting from the very small diode footprint and the photonic amplification from the half-ellipsoidal tapered silicon resonator, the device shows a very high output power density and spectral output power density of 600 mW cm^{-2} and 8 mW cm^{-2} nm^{-1}, respectively. The results, thus, indicate that the proposed device constitutes a significant step ahead towards a silicon light source with a defined spectral characteristic for silicon photonics on a CMOS platform. Such light emitters could be used as a versatile light source for on-chip optical links or for on-chip bio-/chemical sensing applications. Further improvements of these Si-LEDs will involve an increased efficiency and an extension of the emission spectrum towards the NIR (C-band 1400–1600 nm) with strategies such as optical doping, quantum dots, or dislocation engineering.[8,14,27,38] The operation voltage of the proposed Si-based emitter of 1.7 V could be further decreased below 1 V by improving the series resistance originating from the electrical contact on top of the resonator. Finally, strategies to collect the light in a specific direction in such an integrated on-chip light source could be developed with lateral evanescent field coupling to a waveguide as realized, e.g., for some III–V disk lasers.

SUPPLEMENTARY MATERIAL

See the supplementary material for further details on sample fabrication, electrical and optical measurements, experimental data analysis, and numerical simulations. In addition, a comparison of the key parameters of the presented Si-LED to the state-of-the-art in the literature is shown.

DATA AVAILABILITY

The data that support the findings of this study are available from the corresponding author upon reasonable request.

REFERENCES

1. D. Liang and J. E. Bowers, Nat. Photonics **4**, 511 (2010).
2. R. Chen, T.-T. D. Tran, K. W. Ng, W. S. Ko, L. C. Chuang, F. G. Sedgwick, and C. Chang-Hasnain, Nat. Photonics **5**, 170 (2011).
3. D. Saxena, S. Mokkapati, P. Parkinson, N. Jiang, Q. Gao, H. H. Tan, and C. Jagadish, Nat. Photonics **7**, 963 (2013).
4. F. Priolo, T. Gregorkiewicz, M. Galli, and T. F. Krauss, Nat. Nanotechnol. **9**, 19 (2014).
5. L. Pavesi, Mater. Today **8**, 18 (2005).
6. L. Pavesi, L. Dal Negro, C. Mazzoleni, G. Franzò, and F. Priolo, Nature **408**, 440 (2000).
7. S. G. Cloutier, P. A. Kossyrev, and J. Xu, Nat. Mater. **4**, 887 (2005).
8. W. L. Ng, M. A. Lourenço, R. M. Gwilliam, S. Ledain, G. Shao, and K. P. Homewood, Nature **410**, 192 (2001).
9. J. Bao, M. Tabbal, T. Kim, S. Charnvanichborikarn, J. S. Williams, M. J. Aziz, and F. Capasso, Opt. Express **15**, 6727 (2007).
10. S. Coffa, S. Lombardo, F. Priolo, G. Franzó, S. U. Campisano, A. Polman, and G. N. van den Hoven, Nuovo Cimento D **18**, 1131 (1996).
11. A. Polman, J. Appl. Phys. **82**, 1 (1997).
12. H.-S. Han, S.-Y. Seo, and J. H. Shin, Appl. Phys. Lett. **79**, 4568 (2001).
13. A. Shakoor, R. Lo Savio, P. Cardile, S. L. Portalupi, D. Gerace, K. Welna, S. Boninelli, G. Franzò, F. Priolo, T. F. Krauss, M. Galli, and L. O'Faolain, Laser Photonics Rev. **7**, 114 (2013).
14. H. Sumikura, E. Kuramochi, H. Taniyama, and M. Notomi, Sci. Rep. **4**, 5040 (2014).
15. M. A. Green, J. Zhao, A. Wang, P. J. Reece, and M. Gal, Nature **412**, 805 (2001).
16. S. Iwamoto, Y. Arakawa, and A. Gomyo, Appl. Phys. Lett. **91**, 211104 (2007).
17. M. Fujita, B. Gelloz, N. Koshida, and S. Noda, Appl. Phys. Lett. **97**, 121111 (2010).
18. S. W. Schmitt, G. Sarau, and S. H. Christiansen, Sci. Rep. **5**, 17089 (2015).
19. S. W. Schmitt, K. Schwarzburg, and C. Dubourdieu, Sci. Rep. **9**, 9024 (2019).
20. C. Roques-Carmes, S. E. Kooi, Y. Yang, A. Massuda, P. D. Keathley, A. Zaidi, Y. Yang, J. D. Joannopoulos, K. K. Berggren, I. Kaminer, and M. Soljacic, Nat. Commun. **10**, 3176 (2019).
21. F. Chiodi, S. L. Bayliss, L. Barast, D. Débarre, H. Bouchiat, R. H. Friend, and A. D. Chepelianskii, Nat. Commun. **9**, 398 (2018).
22. M. R. Foreman, J. D. Swaim, and F. Vollmer, Adv. Opt. Photonics **7**, 168 (2015).
23. H.-C. Lee and C.-K. Liu, Solid-State Electron. **49**, 1172 (2005).
24. Z. Cheng, C. Ríos, W. H. P. Pernice, C. David Wright, and H. Bhaskaran, Sci. Adv. **3**, e1700160 (2017).
25. J. Y. Mao, L. Zhou, X. Zhu, Y. Zhou, and S. T. Han, Adv. Opt. Mater. **7**, 1900766 (2019).
26. V. Agarwal, S. Dutta, A. J. Annema, R. J. E. Hueting, J. Schmitz, M. J. Lee, E. Charbon, and B. Nauta, in Technical Digest—International Electron Devices Meeting (IEDM), 2019.
27. B. Zheng, J. Michel, F. Y. G. Ren, L. C. Kimerling, D. C. Jacobson, and J. M. Poate, Appl. Phys. Lett. **64**, 2842 (1994).
28. B. P. van Drieënhuizen and R. F. Wolffenbuttel, Sens. Actuators, A **31**, 229 (1992).
29. M. Du Plessis, H. Aharoni, and L. W. Snyman, IEEE J. Sel. Top. Quantum Electron. **8**, 1412 (2002).
30. T. Hoang, P. LeMinh, J. Holleman, and J. Schmitz, in *Proceedings of 35th European Solid-State Device Research Conference (ESSDERC)* (IEEE, 2005), p. 359.
31. A. Khanmohammadi, R. Enne, M. Hofbauer, and H. Zimmermann, in *Proceedings of 45th European Solid-State Device Research Conference (ESSDERC)* (IEEE, 2015), p. 138.
32. K. Cheng, R. Anthony, U. R. Kortshagen, and R. J. Holmes, Nano Lett. **11**, 1952 (2011).
33. E. M. Purcell, Phys. Rev. **69**, 674 (1946).

© Author(s) 2020

[34] S. W. Schmitt, G. Brönstrup, G. Shalev, S. K. Srivastava, M. Y. Bashouti, G. H. Döhler, and S. H. Christiansen, Nanoscale **6**, 7897 (2014).
[35] J. Olivero and R. Longbothum, J. Quant. Spectrosc. Radiat. Transfer **17**, 233 (1977).
[36] M. W. Yim and R. J. Pfaff, J. Appl. Phys. **45**, 1456 (1974).
[37] H. H. Li, J. Phys. Chem. Ref. Data **9**, 561 (1980).
[38] V. Rutckaia, F. Heyroth, A. Novikov, M. Shaleev, M. Petrov, and J. Schilling, Nano Lett. **17**, 6886 (2017).

© Author(s) 2020